NIH Public Access
Author Manuscript
Sci Signal. Author manuscript; available in PMC 2013 February 06.

Published in final edited form as:
Sci Signal. ; 5(231): ra47. doi:10.1126/scisignal.2002712.

Perinuclear Mitochondrial Clustering Creates an Oxidant-Rich Nuclear Domain Required for Hypoxia-Induced Transcription

Abu-Bakr Al-Mehdi[1,2], **Viktor M. Pastukh**[1,2], **Brad M. Swiger**[1,2], **Darla J. Reed**[1,2], **Mita R. Patel**[1,2], **Gina C. Bardwell**[1,2], **Viktoriya V. Pastukh**[1,2], **Mikhail F. Alexeyev**[2,3], and **Mark N. Gillespie**[1,2,*]

[1]Department of Pharmacology, College of Medicine, University of South Alabama, Mobile, AL 36688, USA

[2]Center for Lung Biology, College of Medicine, University of South Alabama, Mobile, AL 36688, USA

[3]Department of Cell Biology and Neuroscience, College of Medicine, University of South Alabama, Mobile, AL 36688, USA

Abstract

Mitochondria can govern local concentrations of second messengers, such as reactive oxygen species (ROS), and mitochondrial translocation to discrete subcellular regions may contribute to this signaling function. Here, we report that exposure of pulmonary artery endothelial cells to hypoxia triggered a retrograde mitochondrial movement that required microtubules and the microtubule motor protein dynein and resulted in the perinuclear clustering of mitochondria. This subcellular redistribution of mitochondria was accompanied by the accumulation of ROS in the nucleus, which was attenuated by suppressing perinuclear clustering of mitochondria with nocodazole to destabilize microtubules or with small interfering RNA–mediated knockdown of dynein. Although suppression of perinuclear mitochondrial clustering did not affect the hypoxia-induced increase in the nuclear abundance of hypoxia-inducible factor 1α (HIF-1α) or the binding of HIF-1α to an oligonucleotide corresponding to a hypoxia response element (HRE), it eliminated oxidative modifications of the *VEGF* (vascular endothelial growth factor) promoter. Furthermore, suppression of perinuclear mitochondrial clustering reduced HIF-1α binding to the *VEGF* promoter and decreased *VEGF* mRNA accumulation. These findings support a model for hypoxia-induced transcriptional regulation in which perinuclear mitochondrial clustering results in ROS accumulation in the nucleus and causes oxidative base modifications in the *VEGF* HRE that are important for transcriptional complex assembly and *VEGF* mRNA expression.

INTRODUCTION

Hypoxia (low oxygen) is a fundamental pathophysiological stimulus, serving as a critical determinant of organogenesis in the developing fetus as well as an inciting factor in normal and tumor angiogenesis and in hypertensive pulmonary vascular remodeling, for example (1). Not surprisingly, considerable effort has been directed toward understanding

*To whom correspondence should be addressed. mgillesp@southalabama.edu.

SUPPLEMENTARY MATERIALS
www.sciencesignaling.org/cgi/content/full/5/231/ra47/DC1

Author contributions: A.-B.A.-M. designed the experiments, interpreted the data, and co-wrote the manuscript; V.M.P., B.M.S., D.J.R., M.R.P., and G.C.B. contributed to the experimental design and executed the experiments; V.V.P. and M.F.A. prepared and evaluated genetic constructs; and M.N.G. designed the experiments, interpreted the data, and co-wrote the manuscript.

Competing interests: The authors declare that they have no competing interests.

NIH-PA Author Manuscript
NIH-PA Author Manuscript
NIH-PA Author Manuscript

NIH-PA Author Manuscript

NIH-PA Author Manuscript

NIH-PA Author Manuscript

mechanisms of hypoxia-related signal transduction. Studies in multiple cell types suggest that hypoxia-induced generation of reactive oxygen species (ROS) by mitochondria plays a key role in this process (2, 3). Details of the pathway have yet to be elucidated, but complex III of the mitochondrial electron transport chain is a probable source of the enhanced generation of ROS (4), which have been linked to calcium mobilization and contraction of pulmonary vascular smooth muscle cells and to stabilization of hypoxia-inducible factor 1α (HIF-1α), the master transcriptional regulator of hypoxic responses (5–7). There are also several reports that hypoxia-generated ROS oxidize specific bases in hypoxia response elements (HREs) of hypoxia-inducible genes (8–10). On the basis of multiple lines of indirect evidence (10–12), it has been speculated that hypoxia-induced base modifications might contribute to transcriptional regulation (13, 14). However, direct support for this concept has been difficult to obtain because current antioxidant strategies fail to discriminate between ROS-mediated accumulation of HIF-1α and the oxidative modifications of critical bases within HREs to which HIF-1α binds to initiate transcription.

Mitochondria are motile organelles (15). Differential distribution of mitochondria in various cell types under defined conditions suggests a functional role for mitochondrial motility (16). Mitochondrial redeployment can be subplasmalemmal, pan-cytoplasmic, or perinuclear (17–19). Subplasmalemmal translocation in immunologically stimulated T lymphocytes enables mitochondria to function as a local calcium sink that modulates calcium channel activity in the cell membrane (20). In the cytoplasm, mitochondrial proximity to the endoplasmic reticulum (ER) governs the dynamics of calcium release from the ER (21). Axonal transport of mitochondria enriches nodes of Ranvier in adenosine 5′-triphosphate (ATP) and other messengers required for neuronal function (22). Finally, perinuclear mitochondrial clustering, which is sometimes asymmetric in nature (23), has been observed during herpes simplex virus infection (24), oocyte fertilization, and embryonic development (17–19). Specific patterns of perinuclear mitochondrial aggregation and microtubule disposition in the cells of the early embryo are related, and asymmetrical mitochondrial distributions at the pronuclear stage can result in some proportion of blastomeres with reduced mitochondrial inheritance and diminished capacity to generate ATP (25). However, little is known about the physiological role of perinuclear mitochondrial clustering.

In light of the possibility that mitochondrial translocation is physiologically important and that mitochondria may serve an important signaling role in hypoxia, we determined whether hypoxia altered subcellular mitochondrial distribution in intact, perfused lungs and in main pulmonary artery endothelial cells (PAECs). After finding that hypoxia caused substantial perinuclear mitochondrial clustering, we next explored the biological relevance of this directed mitochondrial movement. Our results point to previously unappreciated aspects of hypoxic signaling in which the directed translocation of mitochondria to perinuclear regions enriches the nucleus in ROS, which cause targeted base modifications in the *VEGF* (vascular endothelial growth factor) HRE that are important for activation of *VEGF* mRNA transcription.

RESULTS

Hypoxia-initiated and microtubule- and dynein-dependent perinuclear clustering of mitochondria

Initial experiments determined whether hypoxia caused mitochondrial redistribution in the intact lung. In subpleural capillary endothelial cells in the isolated, perfused rat lung ventilated under normoxic conditions, MitoTracker staining showed a diffuse mitochondrial distribution without prominent localization in any subcellular domain (Fig. 1A). However, 3 hours of hypoxic ventilation caused bipolar perinuclear mitochondrial clustering in capillary endothelium.

NIH-PA Author Manuscript

NIH-PA Author Manuscript

NIH-PA Author Manuscript

To develop a model system suitable for exploring the functional importance of hypoxia-induced mitochondrial movement, we evaluated the distribution of mitochondria in normoxic and hypoxic rat cultured PAECs. In normoxic cells, mitochondria were distributed diffusely throughout the cytosol (Fig. 1B). After hypoxic exposure, a perinuclear ring of mitochondria was evident. Mitochondrial translocation to the perinuclear region was evident within 1 hour of hypoxia, more prominent at 3 hours of hypoxic exposure, and sustained for 6 hours of continued hypoxia (Fig. 1C). To determine whether hypoxia altered the pancytoplasmic distribution of mitochondria, we quantified MitoTracker fluorescence in concentric rings radiating outward from the nucleus in normoxic and hypoxic PAECs and calculated the proportion of fluorescence signals as a percentage of the total. The hypoxia-induced increase in the proportion of mitochondrial fluorescence in regions closest to the nucleus was accompanied by a decrease in peripheral mitochondrial deposition (Fig. 1D). Finally, to ascertain whether these effects of hypoxia on mitochondrial distribution were cell type–specific, we applied the same analytical strategy to rat cultured pulmonary artery smooth muscle cells (PASMCs), another important effector cell population in the pulmonary arterialwall that responds to hypoxia with transcriptional activation of critical adaptive genes. In this cell type, hypoxia also caused a prominent redistribution of mitochondria from the peripheral cytosol to the perinuclear region (Fig. 1E). These alterations in the distribution of mitochondria in PAECs and PASMCs were unrelated to changes in cytoskeletal integrity because microtubule morphologies in normoxic and hypoxic cells appeared to be indistinguishable, although there was mitochondrial fragmentation in hypoxic cells, as has been previously reported (26) (fig. S1A).

Because mitochondria are transported along microtubule tracks, we next determined whether destabilization of microtubules with nocodazole would prevent redistribution of mitochondria initiated by hypoxia. Fluorescence microscopic assessment of normoxic and hypoxic cells treated with nocodazole revealed loss of microtubule integrity, in contrast to the netlike pattern seen in control cells (fig. S1B). Although it did not alter the pan-cellular deposition of mitochondria in normoxic cells, nocodazole prevented hypoxia-induced redistribution of mitochondria from the peripheral cytoplasm to the perinuclear region (Fig. 1F).

To isolate the role of retrograde mitochondrial movement in hypoxia-induced perinuclear clustering, we transfected PAECs with a small interfering RNA (siRNA) directed against the heavy chain of dynein (fig. S1C) to inhibit the dynein molecular motor that drives mitochondria toward microtubule organizing centers (16). The microtubule morphology of dynein-deficient cells was indistinguishable from that of controls (fig. S1D). Dynein deficiency in normoxic cells was associated with increased mitochondrial density in the peripheral cytoplasm and reduced mitochondrial localization in the perinuclear region (Fig. 1G). Such a perinuclear-to- peripheral cytosolic shift could be due to the unopposed action of the kinesin motor system in transporting mitochondria on intact microtubule tracks toward the peripheral cytoplasm. Moreover, dynein deficiency inhibited hypoxia-induced perinuclear mitochondrial clustering. Transfection with a scrambled siRNA did not appear to affect mitochondrial distribution in normoxic or hypoxic PAECs. Collectively, these observations in nocodazole-treated and dynein-knockdown cells indicate that hypoxia activates a microtubule- and dynein-dependent pathway directing mitochondria to cluster in close proximity to the nucleus.

ROS originating in part from mitochondrial complex III play a central role in hypoxic signal transduction by triggering calcium mobilization, HIF-1α stabilization, and other effects relevant to adaptation to a low-oxygen environment (2, 27–29). To determine whether perinuclear mitochondrial clustering was a ROS-mediated signaling event in hypoxic cells, we used the complex III inhibitor myxothiazol. Myxothiazol prevented hypoxia-induced

NIH-PA Author Manuscript

NIH-PA Author Manuscript

NIH-PA Author Manuscript

perinuclear mitochondrial clustering (fig. S2A) and did not appear to affect microtubule morphology (fig. S2B). To confirm these findings, we used a nonselective antioxidant, *N*-acetylcysteine. Like myxothiazol, *N*-acetylcysteine also suppressed hypoxia-induced perinuclear mitochondrial clustering (fig. S2C) but did not appear to affect microtubule integrity (fig. S2D). In contrast, antimycin A, which enhances ROS production from complex III (30), failed to alter the distribution of mitochondria (fig. S2E). Collectively, these observations suggest that ROS generation, probably by complex III, is necessary but not sufficient to initiate perinuclear mitochondrial clustering in hypoxic PAECs.

Impact of mitochondrial distribution on hypoxia-induced pan-cellular and nuclear ROS stress

Because mitochondria have been implicated as an important source of ROS in hypoxic signaling, perinuclear clustering of mitochondria in response to hypoxia could be associated with changes in the cellular distribution of ROS. To address this possibility, we transfected cells with nontargeted redox-sensitive green fluorescent protein (roGFP) (31, 32). roGFP contains double-cysteine substitutions that generate a disulfide bond that reacts to oxidants and reductants in a manner similar to that of glutathione disulfide and alters the emission intensity at 510 nm when the probe is excited at 400 and 480 nm (31). The 400-nm excitation/510-nm emission of roGFP increases with increasing oxidant concentrations, and the 480-nm excitation/510-nm emission decreases with increasing oxidant concentrations. The ratiometric fluorescence from two excitation wavelengths enables time-dependent quantitative determinations of ROS in any part of the cell irrespective of local concentration heterogeneity and has been used to detect ROS in vascular smooth muscle and other cells (3, 33). Our initial studies demonstrated that the probe distributes diffusely throughout cytoplasmic and nuclear domains (fig. S3A) and that its dynamic range can be verified with the oxidant *tert*-butyl hydroperoxide and the reducing agent dithiothreitol (DTT) (fig. S3B), as previously described (3).

Next, we examined the actions of hypoxia on spatiotemporal changes in redox state in control PAECs and cells with mitochondrial movement disrupted with nocodazole or dynein knockdown. In normoxic cells, the nucleus was slightly less oxidized compared with the cytosol. Hypoxia increased the accumulation of ROS in both the nuclear and the cytoplasmic regions (Fig. 2, A to C). Inhibition of perinuclear mitochondrial clustering with either nocodazole (Fig. 2, A and B) or dynein silencing (Fig. 2, A and C) exerted identical effects on the hypoxia-induced changes in ROS generation: The roGFP signal was enhanced in the cytosol but suppressed in the nuclear domain (Fig. 2, A to C). Thus, blocking the perinuclear clustering of mitochondria attenuated the accumulation of ROS in the nucleus but not in the cytosol.

The disposition of ROS generation in hypoxia as revealed by roGFP resembled in general aspects the intensity plot analyses of dichlorofluorescein diacetate (DCF-DA) fluorescence (fig. S4A). The fluorescence of DCF increases with increasing oxidant concentration in an irreversible and cumulative manner. DCF fluorescence was detectable in the perinuclear and cytosolic regions in normoxic cells but absent in the nuclear domain. In contrast, PAECs cultured under hypoxic conditions for 60 min displayed increased DCF fluorescence in the cytoplasm but more prominently in the perinuclear and nuclear regions. In addition, myxothiazol abolished the increased ROS abundance in both the nucleus and the cytoplasm, thus confirming previous observations that complex III is an important source of ROS production in hypoxic cells (28). In hypoxic cells, disruption of perinuclear mitochondrial clustering with nocodazole treatment or dynein-specific siRNA abrogated the strong nuclear DCF signal but did not affect DCF fluorescence in the cytoplasm. Indeed, quantification of the pan-cellular DCF signal revealed that neither intervention to suppress perinuclear mitochondrial clustering significantly diminished the hypoxia-induced pan-cellular ROS

NIH-PA Author Manuscript

NIH-PA Author Manuscript

NIH-PA Author Manuscript

production (fig. S4, B and C). Collectively, these findings with roGFP and DCF indicate that the ability of hypoxia to initiate ROS production in the cytosol remained intact when perinuclear mitochondrial clustering was blocked.

These observations suggested that perinuclear mitochondrial clustering in hypoxia is linked to formation of an oxidant-rich nuclear signaling environment. To explore this idea, we used three different approaches to define the actions of nocodazole and dynein knockdown on compartmentalized nuclear oxidative stress in hypoxia. The first method used PAECs that were transfected with an adenoviral construct encoding nuclear-targeted roGFP (fig. S5A). Oxidative or reductive stresses induced by *tert*-butyl hydroperoxide or DTT, respectively, caused spatially similar changes in roGFP signals in the nuclei of PAECs, with changes from baseline more prominent in the nuclear periphery than in the central nucleus (fig. S5B). Hypoxia increased ROS production more prominently in the nuclear periphery than in central nuclear regions (Fig. 3A). Quantification of the hypoxia-induced nuclear roGFP signal demonstrated that the increase in ROS production was evident after 30 min of hypoxic exposure, peaked at 90 min, and persisted for at least 3 hours (Fig. 3B). Suppression of perinuclear mitochondrial clustering with nocodazole (Fig. 3C) or dynein knockdown (Fig. 3D) blocked the increased ROS production in hypoxic PAECs but did not affect ROS production in normoxic PAECs.

Previous studies demonstrated that the ROS production associated with hypoxia caused oxidative base modifications in HREs of hypoxia-inducible genes but not in functionally irrelevant promoter sequences or in promoters of genes whose expression was decreased or not altered by hypoxia (8–11). Accordingly, as a second means to determine whether perinuclear mitochondrial clustering created an oxidant-rich nuclear environment, we measured changes in the density of oxidative base modifications in HRE sequences of the *VEGF*, *NOS2*, and *NFKB2* promoters in control PAECs and in cells treated with nocodazole or transfected with dynein siRNAs to disrupt the mitochondrial movement. The *VEGF* gene was of particular interest because it is a prototypical activation marker of the hypoxia-inducible transcriptional program and because deficient VEGF expression alters organ and vascular structure (34). Lesion densities assessed by polymerase chain reaction (PCR) amplification of the *VEGF* HRE in the absence and presence of pretreatment with the bacterial DNA repair enzyme formamidopyrimidine DNA glycosylase (Fpg) confirmed that hypoxia caused oxidative base modifications in the *VEGF* HRE (8, 9) (Fig. 4). Nocodazole treatment (Fig. 4A) or dynein knockdown (Fig. 4B) inhibited the increase in *VEGF* HRE lesion density in hypoxic PAECs. HREs of the *NOS2* and *NFKB2* promoters also displayed Fpg-sensitive oxidative base modifications in hypoxia that were abrogated when perinuclear mitochondrial clustering was blocked by either nocodazole treatment or dynein knockdown (fig. S6).

As a third strategy, chromatin immunoprecipitation (ChIP) analysis was used to quantify *VEGF* HRE sequences harboring the common base oxidation product 8-oxoguanine in normoxic and hypoxic PAECs. The outcome of these analyses mirrored those of the Fpg-based DNA damage assay. The increase in *VEGF* HRE sequences with 8-oxoguanine in hypoxic PAECs was inhibited by suppression of perinuclear mitochondrial clustering with nocodazole (Fig. 4C) or dynein knockdown (Fig. 4D). 8-Oxoguanine was not detected in a functionally irrelevant *VEGF* promoter sequence located downstream of the HRE under any experimental condition.

Role of nuclear ROS stress in governing HIF-1α –DNA binding and VEGF mRNA expression

Because blockade of perinuclear mitochondrial clustering selectively inhibited the hypoxia-induced increase in nuclear ROS without affecting the increase in cytosolic ROS, we

NIH-PA Author Manuscript

NIH-PA Author Manuscript

NIH-PA Author Manuscript

explored the importance of the oxidant-enriched nuclear domain in hypoxic signaling. We first determined whether disruption of hypoxia-induced mitochondrial clustering and the resulting inhibition of the increase in nuclear ROS affected the distribution of the master transcriptional regulator in hypoxia, HIF-1α. Hypoxia-induced increase in the nuclear abundance of HIF-1α was unaffected by inhibition of perinuclear mitochondrial clustering with nocodazole or dynein knockdown (Fig. 5A). Similarly, the association of nuclear HIF-1α with a 65-mer oligonucleotide fragment of the *VEGF* HRE was insensitive to inhibition of perinuclear mitochondrial clustering (Fig. 5B). However, ChIP analyses indicated that nocodazole treatment (Fig. 5C) or dynein knockdown (Fig. 5D) inhibited the incorporation of HIF-1α into the transcriptional complex forming on the endogenous *VEGF* HRE. This reduction in HIF-1α association with the *VEGF* HRE in hypoxic PAECs was accompanied by inhibition of hypoxia-induced *VEGF* mRNA accumulation (Fig. 5, E and F).

DISCUSSION

The data reported in this paper point to several new, interrelated concepts in hypoxic signaling. First, hypoxia activates a microtubule-dependent and dynein motor-driven mechanism that redistributes mitochondria from the central cytoplasm to the perinuclear region in PAECs. Second, perinuclear mitochondrial clustering in hypoxia is associated with accumulation of nuclear ROS. Finally, the increased nuclear ROS causes oxidative modification in bases in the HRE sequences of the *VEGF* and other gene promoters that, for the *VEGF* HRE, are important for HIF-1α incorporation into the transcriptional complex and *VEGF* mRNA expression.

Because hypoxia causes ROS generation by mitochondrial complex III (2), which leads to oxidative DNA modifications in HREs of transcriptionally active, hypoxia-inducible genes (11), we assessed whether perinuclear mitochondrial clustering was responsible for creation of an oxidant-rich nuclear signaling domain. In support of this idea, hypoxia failed to increase the signal from a nuclear-targeted, redox-sensitive roGFP probe, and nuclear DCF fluorescence was absent when clustering was suppressed by dynein deficiency or microtubule destabilization with nocodazole. Oxidative base modifications evoked by hypoxia in *VEGF*, *NOS2*, and *NFKB2* HREs were also abrogated when perinuclear clustering was suppressed. We did not identify the specific DNA-modifying reactive species generated by mitochondria clustered in the perinuclear region, but only hydrogen peroxide, which is released from mitochondria (35), has a sufficiently long diffusion distance to permit its permeation into the nuclear compartment. Collectively, these observations support the notion that hypoxia-induced perinuclear mitochondrial clustering in PAECs creates a nuclear signaling environment enriched in ROS, which results in the introduction of oxidative base modification in HRE sequences of hypoxia-inducible promoters.

Blockade of the hypoxia-induced increase in nuclear ROS by preventing perinuclear mitochondrial clustering did not suppress ROS generation in the cytosol, nor did it affect the nuclear accumulation or DNA binding activity of HIF-1α. These findings are consistent with the cytoplasmic localization of the ROS-sensitive prolyl hydroxylases responsible for HIF-1α degradation during normoxia (36, 37) and provided an opportunity to discriminate between the cytoplasmic and the nuclear roles of ROS generated during hypoxic signaling. We found that suppression of perinuclear mitochondrial clustering inhibited oxidative base damage in HRE sequences in the *VEGF* and other genes. Moreover, when base damage was prevented, HIF-1α failed to associate with *VEGF* HRE, and *VEGF* mRNA expression was reduced. These observations are important for two general reasons. First, multiple emerging lines of evidence suggest that hypoxia causes mutagenesis (38–40), and the finding that hypoxia-induced perinuclear mitochondrial clustering is accompanied by oxidative

NIH-PA Author Manuscript

NIH-PA Author Manuscript

NIH-PA Author Manuscript

modification of genomic DNA suggests a previously unappreciated mechanism by which mitochondria may contribute to hypoxia-related mutations. Second, the current findings support a new model of hypoxia-induced transcription in which formation of oxidative base modifications at key nucleotides within or near the HRE initiated by ROS produced from perinuclear mitochondria is required for incorporation of HIF-1α into the hypoxia-inducible transcriptional complex forming on the HRE and for mRNA expression.

In some respects, this model is similar to that described for activation of the *pS2*, *BCL-2*, and *c-MYC* genes by estrogen receptor-α in MCF-7 cells. Ligation and DNA binding of the estrogen receptor-α to estrogen-responsive elements (EREs) recruits lysine-specific demethylase-1 (LSD-1). Local hydrogen peroxide generation by chromatin-bound LSD-1 causes oxidative base damage, which in turn leads to transient strand cleavage because of base excision repair of the lesion (41–43) or recruitment of the strand-cleaving topoisomerase IIβ (44). Formation and repair of strand breaks is thus associated with chromatin remodeling and results in transient changes in DNA conformation required for transcriptional activation (42, 43, 45). Although less information is available concerning the role of oxidative DNA modifications in hypoxic transcription, studies using an oligonucleotide model of the *VEGF* HRE show that incorporation of an abasic site at the guanine modified in hypoxia increases HIF-1α–DNA binding and elicits more robust reporter gene expression (10). In addition, the presence of an apurinic/apyrimidinic site in a model *VEGF* HRE leads to APE1/Ref-1–dependent strand cleavage and increased flexibility of the otherwise rigid HRE sequence (12). Collectively, these observations suggest that sequence-specific base oxidation is important for transcription, at least in part, because the process of lesion repair alters the mechanical properties of DNA.

How sequence-specific lesion formation interacts with transcription factor binding is less clear. In transformed cells, binding of liganded estrogen receptor-α to the ERE triggers the recruitment of LSD-1 and subsequent base modifications (42, 43). By contrast, in hypoxic PAECs, persistent incorporation of HIF-1α into the transcriptional complex forming on the *VEGF* HRE appears to be a consequence rather than a cause of lesion formation. The basis and meaning of these differences are unknown, but one possibility is that pathways leading to increased nuclear ROS, base oxidation and repair, and transcriptional complex assembly may be cell- and stimulus-specific. It should also be noted that discrete ROS sources may interact and that ROS derived from perinuclear mitochondria may activate enzymatic (for example, LSD-1) and nonenzymatic pathways (for example, iron mobilization) that serve as direct causes of sequence-specific base modifications.

The observation that suppression of hypoxia-induced ROS generation by two disparate pharmacologic agents—myxothiazol, which inhibits ROS production by complex III, and the nonselective ROS scavenger, *N*-acetylcysteine—attenuated perinuclear mitochondrial clustering raises the possibility that mitochondria-generated ROS initiate movement of the organelle to the perinuclear region. In support of this idea, some endogenous modulators of dynein- and kinesin-dependent mitochondrial movement contain redox-sensitive sulfhydryl groups (46) through which hypoxia-derived ROS could modulate mitochondrial distribution (47). However, antimycin A, which increases ROS formation by complex III in the absence of hypoxia, did not initiate mitochondrial perinuclear clustering, indicating that hypoxia-induced ROS production from complex III is necessary but not sufficient for the clustering response. Hypoxia caused mitochondrial fragmentation, as reported previously (26). The demonstration that *drp1*-mediated mitochondrial fragmentation or fission is associated with perinuclear clustering (48) raises the intriguing prospect that hypoxia or other physiologic signals initiate retrograde movement through interactive processes using both mitochondria-generated ROS and fission of mitochondria. Additional experiments will be required to

NIH-PA Author Manuscript

NIH-PA Author Manuscript

NIH-PA Author Manuscript

elucidate the mechanism by which mitochondrial-derived ROS contributes to hypoxia-induced perinuclear mitochondrial clustering.

In summary, we show that hypoxia causes perinuclear mitochondrial clustering in intact lungs and cultured PAECs. Experiments in cultured cells revealed that the dynein motor system operating in concert with microtubules played a critical role in the hypoxia-directed perinuclear clustering of mitochondria. Disruption of the clustering response did not affect cytosolicROS but suppressed the increase in nuclear ROS and oxidative base modifications in the *VEGF*HRE. Under these conditions, HIF-1α accumulated in the nucleus but failed to associate with the endogenous *VEGF* HRE or to initiate *VEGF* mRNA expression. Collectively, these findings support a new paradigm for hypoxic signaling in which controlled oxidative base modifications in HREs of hypoxia-inducible genes, initiated byROS generated frommitochondria clustering in close proximity to the nucleus, play an important role in transcriptional activation.

MATERIALS AND METHODS

Isolated, perfused rat lung

To study mitochondrial disposition in endothelial cells in situ, we used an established intact lung microscopy method (49, 50). Briefly, after isolation, the lung was perfused with MitoTracker Deep Red 633 (100 nM) by a pump through the pulmonary artery with Krebs-Ringer bicarbonate solution with 5% dextran and 10 mM glucose at pH 7.4 for 30 min with normoxic ventilation. After dye washout for 5 min, the lungs were placed in a specially designed Plexiglas chamber with a coverslip window at the bottom so that the posterior surface of the lung gently touched the coverslip. Lungs were then ventilated for 3 hours with either 5% CO_2+ 95% air (normoxia) or 5% CO_2 + 93% N_2 + 2%O_2 (hypoxia). For three-dimensional (3D) reconstruction, cells in vessels were imaged by optical slicing along 40 μm of *z* axis at 0.5-μm intervals. The PSF-deconvolved stacks of images were used to create noise-free 3D reconstructions to determine the distribution pattern of mitochondria in the endothelial cells.

Pulmonary artery endothelial cell culture, hypoxic exposure, and VEGF mRNA expression

Rat PAECs and PASMCs, isolated and cultured as described previously (8, 51, 52), were used between passages 9 and 18. For culture in normoxia or hypoxia, 60-mm petri plates were placed in an incubator purged with either 21 or 2% O_2, respectively. *VEGF* mRNA expression, used as a prototypical activation marker of the hypoxia-induced transcriptional program in PAECs, was determined by quantitative real-time PCR, also as described previously (9). Briefly, total RNAwas isolated from PAECs with the PrepEase RNA Spin Kit (USB) according to the manufacturer's protocol. Quantitative real-time PCR was then performed with the HotStart-IT SYBR Green One-Step qRT-PCRKit (USB), also according to themanufacturer's protocol. Primers used in the quantitative reverse transcription–PCR (qRT-PCR) analyses of *VEGF* mRNA expression were 5′-ATCTCTTGCTCTTTCTTA-3′ (forward) and 5′-AATATCTTCTCAGGACAA-3′ (reverse). For normalization of*VEGF*mRNAexpression, 28*S* ribosomalRNA(rRNA)was amplified with the following primers: 5′-CTCAACCTATTCTCAAAC-3′ (forward) and 5′-GTCTATATCAACCAACAC-3′ (reverse).

Analysis and modulation of mitochondrial distribution in PAECs

Rat PAECs labeled with MitoTracker Deep Red 633 (100 nM) were placed in a chamber controlled for partial pressure of oxygen (PO_2), partial pressure of CO_2 (P_{CO_2}), and temperature (53). Time-lapse pictures at intervals of 15 min for up to 3 hours were acquired in both the fluorescence and differential interference contrast (DIC) channels. The DIC

NIH-PA Author Manuscript

NIH-PA Author Manuscript

NIH-PA Author Manuscript

pictures were used to calculate the distance of peripheral mitochondria from the edge of the cell and for determination of the effect of possible cell shrinkage on the mitochondrial translocation. Nuclear labeling was done at the end of the experiment with Hoechst 33342 (10 μM). Adding the nuclear dye at the beginning and imaging the nucleus at each mitochondrial acquisition was unnecessary because the shape and volume of nuclei did not appear to substantially change with hypoxia. Addition of Hoechst 33342 at the end of the experiment prevented the potential cytotoxicity and phototoxicity associated with its DNA-intercalating properties and the requirement of ultraviolet exposure for imaging.

For analysis of clustering, the MitoTracker signal in pictures from each time point was segmented into nucleocentric rings of equal width from the margin of the nucleus toward the periphery of the cells and inside the nucleus. Average pixel intensity within each ring indicated the abundance of mitochondrial signal in that ring, and these values were plotted as a function of distance. Initially, the images were calibrated for real-world distance measurements by applying calibration for the objective and other optics by imaging a micrometer. For image segmentation, a binary mask for the nucleus was created by edge detection and thresholding. The edge of the nucleus was converted into the outline of a region of interest. This line was progressively and symmetrically dilated at defined intervals by means of the mathematical transformation “Dilate” of the MetaMorph (Molecular Devices) program. Average intensity values and distances and other parameters were generated by morphometric analysis and data logging functions available in MetaMorph commands. The numerical data files thus generated were subjected to statistical analysis with SigmaStat and SigmaPlot (Systat Inc.). The potential photobleaching effect from repeated exposures for time lapse was eliminated because the total intensity of mitochondrial signal for each image from each time point was taken as 100% and the signal distribution among perinuclear segments was normalized to the total cellular signal. For graphical presentation, the percentage of total cellular mitochondrial signal located in the nuclear ring and its two most proximate concentric zones were pooled, termed the “% mitochondria in perinuclear region,” and depicted as a function of time in hypoxia.

To disrupt microtubule-based mitochondrial movement, we incubated PAECs with the microtubule-destabilizing agent nocodazole at a concentration of 50 nM for 30 min before culture under either normoxic or hypoxic conditions for the indicated durations. Retrograde mitochondrial movement (movement toward the microtubule organizing centers) was suppressed by siRNA-mediated knockdown of the dynein heavy chain, a component of the molecular motor driving this movement. PAECs were transfected with Dharmafect I (Thermo Fisher Scientific) following the manufacturer’s instructions. In brief, cells were seeded at 400,000 per well in six-well plates and transfected the next day with 100 nM siRNA and 2 μl of Dharmafect. Cells were exposed to hypoxia 24 hours after transfection, after which nuclear DNA and RNA were isolated. The efficiency of the siRNA strategy to knock down dynein was confirmed by Western immunoblot analysis with an antibody to DYNC1H1 and quantified by normalizing dynein heavy chain abundance to glyceraldehyde-3-phosphate dehydrogenase (GAPDH) (Santa Cruz Biotechnology). Knockdown efficiency was also confirmed by qRT-PCR analysis of *DYNC1H1* mRNA with the following primers: 5′-CCATCGTCAACTTCTCAG-3′ (forward) and 5′-CTCCACTCGCTTTAACAT-3′ (reverse). Expression was normalized to 28*S* rRNA with the primers noted above.

To determine the effects of nocodazole and dynein knockdown on microtubule morphology, we stained microtubules with Oregon Green paclitaxel. Nuclei were labeled by staining with Hoechst 33342.

NIH-PA Author Manuscript

NIH-PA Author Manuscript

NIH-PA Author Manuscript

Fluorescence microscopic detection of pan-cellular and nuclear oxidative stress

Pan-cellular oxidative stress was monitored by means of two strategies. First, we generated two versions of a redox-sensitive roGFP probe (31, 32): one without a targeting sequence for assessment of pan-cellular ROS stress and the other encoding the nuclear localizing sequence from Minibrain kinase/dual-specificity tyrosine phosphorylation–regulated kinase 1A (54). The nontargeted and nuclear-targeted roGFPs were stably and transiently transfected, respectively, into rat PAECs by standard methods. As a second method of ROS detection, we used DCF-DA–based quantitative fluorescence imaging (55). PAECs were incubated with 5 μM DCF-DA for 30 min to enable dye uptake.

Cells transfected with either nontargeted or nuclear-targeted roGFP constructs or loaded with DCF were subjected to hypoxia (2% oxygen or 30 ± 2.5 mmHg) or normoxia in a temperature-, PO_2-, and P_{CO_2}-controlled chamber for the indicated periods. Time-lapse imaging at 15-min intervals for up to 3 hours was performed for both ROS-detecting probes. For assessment of roGFP signals, we followed a protocol similar to that previously described byWaypa and co-workers (3) in their studies on hypoxia-induced mitochondrial ROS production. PAECs were cultured in normoxia or hypoxia for the indicated periods with ratiometric imaging of roGFP at the indicated times. After hypoxic or normoxic exposure, cells were subsequently challenged with *tert*-butyl hydroperoxide followed by DTT to define the dynamic range of the probe. Because the ratio of fluorescence emissions at 400 and 480 nm, respectively, in normoxic and hypoxic cells was always within the dynamic range of the probe, redox stress evoked by hypoxia was quantified by image segmentation and ratiometric analysis. In some experiments, ratiometric and DIC images were overlaid to demarcate nuclear boundaries, thus enabling discrete quantification of roGFP signals in nuclear and cytoplasmic compartments. For DCF fluorescence, signals were quantified in terms of the change in fluorescence intensity per cell. For visual representation of roGFP and DCF fluorescence, an intensity plot method was used. This method creates pixel-based 3D bar graphs of signal intensity along the *z* axis using the *x* and *y* axes of the dimension of the bottom of the cell itself. The height as well as the pseudo-color of the intensity lines representing each pixel of the cell creates a visual map of ROS distribution throughout the cell.

Detection of oxidative modifications in the *VEGF*, *NOS2*, and *NFKB2* HREs

Hypoxia-induced oxidative base modifications in selected HRE sequences were detected with a previously described PCR-based technique wherein the bacterial DNA glycosylase Fpg (New England Biolabs) was applied to recognize and cleave 8-oxoguanine and related oxidized base products (9, 56). Treatment of DNA with Fpg results in strand cleavage at sites of oxidized purines, thereby creating single-strand breaks that block PCR amplification. Differences in PCR amplification between Fpg-treated and untreated DNA are thus a specific indicator of the presence of oxidative base damage. Aliquot parts containing 10 ng of genomic DNAwith or without pretreatment with Fpg were then subjected to PCR with the following primers to amplify ~200 base pairs (bp) of the following gene promoters harboring HRE sequences: *VEGF*, 5′-GCTCTGCCAGACTCCACAGT-3′ (forward) and 5′-GGCTACGTGGAAGGCAAGTA-3′ (reverse); *NOS2*, 5′-TAACCTGCTGAACTATCT-3′ (forward) and 5′-TACACCAAGTAAGAGTCA- 3′ (reverse); and *NFKB2*, 5′-TGCGCACAGGAACAGAACACTT-3′ (forward) and 5′-TTCATCCCTAATGTCTTGTGTG-3′ (reverse). Data are presented as the percentage of intact DNA; a decrease in the percentage reflects an increase in the number of sequences harboring oxidized base products recognized and cleaved by Fpg.

ChIP analyses were also used to search for *VEGF* HRE sequences harboring the commonly occurring base oxidation product 8-oxoguanine. Commercially available ChIP-IT Express or

NIH-PA Author Manuscript

NIH-PA Author Manuscript

NIH-PA Author Manuscript

ChIP-IT Express Enzymatic kits were used, depending on the specific experiment (Active Motif). Briefly, ~2×10^7 PAECs were fixed with 1% formaldehyde (Sigma) for 10 min and washed with ice-cold 1× phosphate-buffered saline. The fixation reaction was terminated by the addition of Glycine Stop-Fix solution for 5 min. PAECs were washed and collected in Cell Scraping Solution supplemented with 0.5 mM phenylmethylsulfonyl fluoride. Chromatin, sheared to ~500-nucleotide fragments by sonication or by enzymatic shearing, was then immunoprecipitated with specific antibody per manufacturer's instructions. Immunoprecipitated DNA and input DNA controls were amplified by qPCR with HotStart-IT SYBR Green qPCR Kit (USB) and primers specific for the *VEGF* HRE. As a negative control, an ~200-bp sequence 3′ to the HRE, in close proximity to the transcription start site, was amplified after immunoprecipitation.

Determination of nuclear HIF-1α abundance and DNA binding

Nuclear proteins were isolated from normoxic and hypoxic PAECs and divided into two aliquots. Western immunoblot analysis applied to one of the samples was used to determine the abundance of nuclear HIF-1α and the nuclear marker lamin A/C in normoxic and hypoxic PAECs as a function of perinuclear mitochondrial disposition. The abundance of HIF-1α was normalized to that of lamin A/C. The second aliquot was used in DNA affinity precipitation analyses in which nuclear proteins were incubated with a 65-mer sequence of the rat *VEGF* HRE including the HIF-1α DNA recognition site. Subsequently, Western immunoblots were used to determine whether prevention of hypoxia-induced perinuclear mitochondrial clustering altered the ability of HIF-1α to associate with an oligonucleotide model of the *VEGF* HRE. All procedures were performed as described previously (12, 57). ChIP assays, executed as described above, were used to determine the impact of hypoxia-induced changes in perinuclear mitochondrial distribution on HIF-1α association with the endogenous *VEGF* HRE and with a functionally irrelevant promoter sequence closer to the transcription start site.

Statistical analysis

Quantitative data are presented as the means ± SE. Because the data were normally distributed, differences between experimental groups were determined with either a one-way or a two-way analysis of variance (ANOVA), depending on the experimental design, and with Newman-Keuls post hoc test when appropriate. Differences were considered statistically significant when $P < 0.05$.

Supplementary Material

Refer to Web version on PubMed Central for supplementary material.

Acknowledgments

This work was supported by the NIH (R01HL58234, R01HL073244, R01HL113614, 8R01OD010944-03, and Project #3 in P01HL66299).

REFERENCES AND NOTES

1. Sylvester JT, Shimoda LA, Aaronson PI, Ward JP. Hypoxic pulmonary vasoconstriction. Physiol Rev. 2012; 92:367–520. [PubMed: 22298659]
2. Bell EL, Klimova TA, Eisenbart J, Moraes CT, Murphy MP, Budinger GR, Chandel NS. The Q_o site of the mitochondrial complex III is required for the transduction of hypoxic signaling via reactive oxygen species production. J Cell Biol. 2007; 177:1029–1036. [PubMed: 17562787]

NIH-PA Author Manuscript

NIH-PA Author Manuscript

NIH-PA Author Manuscript

3. Waypa GB, Marks JD, Guzy R, Mungai PT, Schriewer J, Dokic D, Schumacker PT. Hypoxia triggers subcellular compartmental redox signaling in vascular smooth muscle cells. Circ Res. 2010; 106:526–535. [PubMed: 20019331]
4. Bell EL, Chandel NS. Mitochondrial oxygen sensing: Regulation of hypoxia-inducible factor by mitochondrial generated reactive oxygen species. Essays Biochem. 2007; 43:17–27. [PubMed: 17705790]
5. Bell EL, Klimova TA, Eisenbart J, Schumacker PT, Chandel NS. Mitochondrial reactive oxygen species trigger hypoxia-inducible factor-dependent extension of the replicative life span during hypoxia. Mol Cell Biol. 2007; 27:5737–5745. [PubMed: 17562866]
6. Semenza GL. Regulation of metabolism by hypoxia-inducible factor 1. Cold Spring Harb Symp Quant Biol. 2011; 76:347–353. [PubMed: 21785006]
7. Desireddi JR, Farrow KN, Marks JD, Waypa GB, Schumacker PT. Hypoxia increases ROS signaling and cytosolic Ca^{2+} in pulmonary artery smooth muscle cells of mouse lungs slices. Antioxid Redox Signal. 2010; 12:595–602. [PubMed: 19747064]
8. Grishko V, Solomon M, Breit JF, Killilea DW, Ledoux SP, Wilson GL, Gillespie MN. Hypoxia promotes oxidative base modifications in the pulmonary artery endothelial cell VEGF gene. FASEB J. 2001; 15:1267–1269. [PubMed: 11344109]
9. Pastukh V, Ruchko M, Gorodnya O, Wilson GL, Gillespie MN. Sequence-specific oxidative base modifications in hypoxia-inducible genes. Free Radic Biol Med. 2007; 43:1616–1626. [PubMed: 18037127]
10. Ziel KA, Grishko V, Campbell CC, Breit JF, Wilson GL, Gillespie MN. Oxidants in signal transduction: Impact on DNA integrity and gene expression. FASEB J. 2005; 19:387–394. [PubMed: 15746182]
11. Ruchko MV, Gorodnya OM, Pastukh VM, Swiger BM, Middleton NS, Wilson GL, Gillespie MN. Hypoxia-induced oxidative base modifications in the VEGF hypoxia-response element are associated with transcriptionally active nucleosomes. Free Radic Biol Med. 2009; 46:352–359. [PubMed: 18992807]
12. Breit JF, Ault-Ziel K, Al-Mehdi AB, Gillespie MN. Nuclear protein-induced bending and flexing of the hypoxic response element of the rat vascular endothelial growth factor promoter. FASEB J. 2008; 22:19–29. [PubMed: 17766324]
13. Gillespie MN, Pastukh V, Ruchko MV. Oxidative DNA modifications in hypoxic signaling. Ann N Y Acad Sci. 2009; 1177:140–150. [PubMed: 19845616]
14. Gillespie MN, Pastukh VM, Ruchko MV. Controlled DNA “damage” and repair in hypoxic signaling. Respir Physiol Neurobiol. 2010; 174:244–251. [PubMed: 20831905]
15. Forman DS, Lynch KJ, Smith RS. Organelle dynamics in lobster axons: Anterograde, retrograde and stationary mitochondria. Brain Res. 1987; 412:96–106. [PubMed: 3607465]
16. Frederick RL, Shaw JM. Moving mitochondria: Establishing distribution of an essential organelle. Traffic. 2007; 8:1668–1675. [PubMed: 17944806]
17. Tarazona AM, Rodriguez JI, Restrepo LF, Olivera-Angel M. Mitochondrial activity, distribution and segregation in bovine oocytes and in embryos produced in vitro. Reprod Domest Anim. 2006; 41:5–11. [PubMed: 16420320]
18. Katayama M, Zhong Z, Lai L, Sutovsky P, Prather RS, Schatten H. Mitochondrial distribution and microtubule organization in fertilized and cloned porcine embryos: Implications for developmental potential. Dev Biol. 2006; 299:206–220. [PubMed: 16945363]
19. Bavister BD. The mitochondrial contribution to stem cell biology. Reprod Fertil Dev. 2006; 18:829–838. [PubMed: 17147931]
20. Quintana A, Schwarz EC, Schwindling C, Lipp P, Kaestner L, Hoth M. Sustained activity of calcium release-activated calcium channels requires translocation of mitochondria to the plasma membrane. J Biol Chem. 2006; 281:40302–40309. [PubMed: 17056596]
21. Mironov SL, Ivannikov MV, Johansson M. $[Ca^{2+}]_i$ signaling between mitochondria and endoplasmic reticulum in neurons is regulated by microtubules. From mitochondrial permeability transition pore to Ca^{2+}-induced Ca^{2+} release. J Biol Chem. 2005; 280:715–721. [PubMed: 15516333]

NIH-PA Author Manuscript NIH-PA Author Manuscript NIH-PA Author Manuscript

22. Hollenbeck PJ, Saxton WM. The axonal transport of mitochondria. J Cell Sci. 2005; 118:5411–5419. [PubMed: 16306220]
23. Hallmann A, Milczarek R, Lipiński M, Kossowska E, Spodnik JH, WoŸniak M, Wakabayashi T, Klimek J. Fast perinuclear clustering of mitochondria in oxidatively stressed human choriocarcinoma cells. Folia Morphol. 2004; 63:407–412.
24. Murata T, Goshima F, Daikoku T, Inagaki-Ohara K, Takakuwa H, Kato K, Nishiyama Y. Mitochondrial distribution and function in herpes simplex virus-infected cells. J Gen Virol. 2000; 81:401–406. [PubMed: 10644838]
25. Van Blerkom J, Davis P, Alexander S. Differential mitochondrial distribution in human pronuclear embryos leads to disproportionate inheritance between blastomeres: Relationship to microtubular organization, ATP content and competence. Hum Reprod. 2000; 15:2621–2633. [PubMed: 11098036]
26. Archer SL, Gomberg-Maitland M, Maitland ML, Rich S, Garcia JG, Weir EK. Mitochondrial metabolism, redox signaling, and fusion: A mitochondria-ROS-HIF-1α-Kv1.5 O_2-sensing pathway at the intersection of pulmonary hypertension and cancer. Am J Physiol Heart Circ Physiol. 2008; 294:H570–H578. [PubMed: 18083891]
27. Comito G, Calvani M, Giannoni E, Bianchini F, Calorini L, Torre E, Migliore C, Giordano S, Chiarugi P. HIF-1α stabilization by mitochondrial ROS promotes Metdependent invasive growth and vasculogenic mimicry in melanoma cells. Free Radic Biol Med. 2011; 51:893–904. [PubMed: 21703345]
28. Guzy RD, Hoyos B, Robin E, Chen H, Liu L, Mansfield KD, Simon MC, Hammerling U, Schumacker PT. Mitochondrial complex III is required for hypoxia-induced ROS production and cellular oxygen sensing. Cell Metab. 2005; 1:401–408. [PubMed: 16054089]
29. Chandel NS, McClintock DS, Feliciano CE, Wood TM, Melendez JA, Rodriguez AM, Schumacker PT. Reactive oxygen species generated at mitochondrial complex III stabilize hypoxia-inducible factor-1α during hypoxia: A mechanism of O_2 sensing. J Biol Chem. 2000; 275:25130–25138. [PubMed: 10833514]
30. Li C, Wright MM, Jackson RM. Reactive species mediated injury of human lung epithelial cells after hypoxia-reoxygenation. Exp Lung Res. 2002; 28:373–389. [PubMed: 12097231]
31. Dooley CT, Dore TM, Hanson GT, Jackson WC, Remington SJ, Tsien RY. Imaging dynamic redox changes in mammalian cells with green fluorescent protein indicators. J Biol Chem. 2004; 279:22284–22293. [PubMed: 14985369]
32. Hanson GT, Aggeler R, Oglesbee D, Cannon M, Capaldi RA, Tsien RY, Remington SJ. Investigating mitochondrial redox potential with redox-sensitive green fluorescent protein indicators. J Biol Chem. 2004; 279:13044–13053. [PubMed: 14722062]
33. Guzy RD, Sharma B, Bell E, Chandel NS, Schumacker PT. Loss of the SdhB, but not the SdhA, subunit of complex II triggers reactive oxygen species-dependent hypoxia-inducible factor activation and tumorigenesis. Mol Cell Biol. 2008; 28:718–731. [PubMed: 17967865]
34. Eichmann A, Simons M. VEGF signaling inside vascular endothelial cells and beyond. Curr Opin Cell Biol. 2012; 24:188–193. [PubMed: 22366328]
35. Boveris A, Valdez LB, Zaobornyj T, Bustamante J. Mitochondrial metabolic states regulate nitric oxide and hydrogen peroxide diffusion to the cytosol. Biochim Biophys Acta. 2006; 1757:535–542. [PubMed: 16615992]
36. Yasumoto K, Kowata Y, Yoshida A, Torii S, Sogawa K. Role of the intracellular localization of HIF-prolyl hydroxylases. Biochim Biophys Acta. 2009; 1793:792–797. [PubMed: 19339211]
37. Cash TP, Pan Y, Simon MC. Reactive oxygen species and cellular oxygen sensing. Free Radic Biol Med. 2007; 43:1219–1225. [PubMed: 17893032]
38. Reynolds TY, Rockwell S, Glazer PM. Genetic instability induced by the tumor microenvironment. Cancer Res. 1996; 56:5754–5757. [PubMed: 8971187]
39. Yuan J, Glazer PM. Mutagenesis induced by the tumor microenvironment. Mutat Res. 1998; 400:439–446. [PubMed: 9685702]
40. Ohno M, Miura T, Furuichi M, Tominaga Y, Tsuchimoto D, Sakumi K, Nakabeppu Y. A genome-wide distribution of 8-oxoguanine correlates with the preferred regions for recombination and

NIH-PA Author Manuscript

NIH-PA Author Manuscript

NIH-PA Author Manuscript

single nucleotide polymorphism in the human genome. Genome Res. 2006; 16:567–575. [PubMed: 16651663]

41. Forneris F, Binda C, Battaglioli E, Mattevi A. LSD1: Oxidative chemistry for multi-faceted functions in chromatin regulation. Trends Biochem Sci. 2008; 33:181–189. [PubMed: 18343668]
42. Amente S, Lania L, Avvedimento EV, Majello B. DNA oxidation drives Myc mediated transcription. Cell Cycle. 2010; 9:3002–3004. [PubMed: 20714214]
43. Perillo B, Ombra MN, Bertoni A, Cuozzo C, Sacchetti S, Sasso A, Chiariotti L, Malorni A, Abbondanza C, Avvedimento EV. DNA oxidation as triggered by H3K9me2 demethylation drives estrogen-induced gene expression. Science. 2008; 319:202–206. [PubMed: 18187655]
44. Ju BG, Lunyak VV, Perissi V, Garcia-Bassets I, Rose DW, Glass CK, Rosenfeld MG. A topoisomerase IIβ-mediated dsDNA break required for regulated transcription. Science. 2006; 312:1798–1802. [PubMed: 16794079]
45. Nunez E, Kwon YS, Hutt KR, Hu Q, Cardamone MD, Ohgi KA, Garcia-Bassets I, Rose DW, Glass CK, Rosenfeld MG, Fu XD. Nuclear receptor-enhanced transcription requires motor- and LSD1-dependent gene networking in interchromatin granules. Cell. 2008; 134:189. [PubMed: 18630350]
46. Harrison A, Sakato M, Tedford HW, Benashski SE, Patel-King RS, King SM. Redox-based control of the γ heavy chain ATPase from *Chlamydomonas* outer arm dynein. Cell Motil Cytoskeleton. 2002; 52:131–143. [PubMed: 12112141]
47. Dewitt DA, Hurd JA, Fox N, Townsend BE, Griffioen KJ, Ghribi O, Savory J. Peri-nuclear clustering of mitochondria is triggered during aluminum maltolate induced apoptosis. J Alzheimers Dis. 2006; 9:195–205. [PubMed: 16873966]
48. Frieden M, James D, Castelbou C, Danckaert A, Martinou JC, Demaurex N. Ca^{2+} homeostasis during mitochondrial fragmentation and perinuclear clustering induced by hFis1. J Biol Chem. 2004; 279:22704–22714. [PubMed: 15024001]
49. Al-Mehdi AB, Zhao G, Dodia C, Tozawa K, Costa K, Muzykantov V, Ross C, Blecha F, Dinauer M, Fisher AB. Endothelial NADPH oxidase as the source of oxidants in lungs exposed to ischemia or high K^+ Circ Res. 1998; 83:730–737. [PubMed: 9758643]
50. Al-Mehdi AB, Tozawa K, Fisher AB, Shientag L, Lee A, Muschel RJ. Intravascular origin of metastasis from the proliferation of endothelium-attached tumor cells: A new model for metastasis. Nat Med. 2000; 6:100–102. [PubMed: 10613833]
51. Killilea DW, Hester R, Balczon R, Babal P, Gillespie MN. Free radical production in hypoxic pulmonary artery smooth muscle cells. Am J Physiol Lung Cell Mol Physiol. 2000; 279:L408–L412. [PubMed: 10926565]
52. Dobson AW, Grishko V, LeDoux SP, Kelley MR, Wilson GL, Gillespie MN. Enhanced mtDNA repair capacity protects pulmonary artery endothelial cells from oxidant-mediated death. Am J Physiol Lung Cell Mol Physiol. 2002; 283:L205–L210. [PubMed: 12060578]
53. Al-Mehdi, AB. Mitochondria: The Dynamic Organelle. Schaffer, SR.; Suleiman, MS., editors. Springer; New York: 2007. p. 169-180.
54. Funakoshi E, Hori T, Haraguchi T, Hiraoka Y, Kudoh J, Shimizu N, Ito F. Overexpression of the human *MNB/DYRK1A* gene induces formation of multinucleate cells through overduplication of the centrosome. BMC Cell Biol. 2003; 4:12. [PubMed: 12964950]
55. al-Mehdi A, Shuman H, Fisher AB. Fluorescence microtopography of oxidative stress in lung ischemia-reperfusion. Lab Invest. 1994; 70:579–587. [PubMed: 8176898]
56. Yankner BA, Lu T. Amyloid β-protein toxicity and the pathogenesis of Alzheimer disease. J Biol Chem. 2009; 284:4755–4759. [PubMed: 18957434]
57. Ziel KA, Campbell CC, Wilson GL, Gillespie MN. Ref-1/Ape is critical for formation of the hypoxia-inducible transcriptional complex on the hypoxic response element of the rat pulmonary artery endothelial cell VEGF gene. FASEB J. 2004; 18:986–988. [PubMed: 15084519]

NIH-PA Author Manuscript
NIH-PA Author Manuscript
NIH-PA Author Manuscript

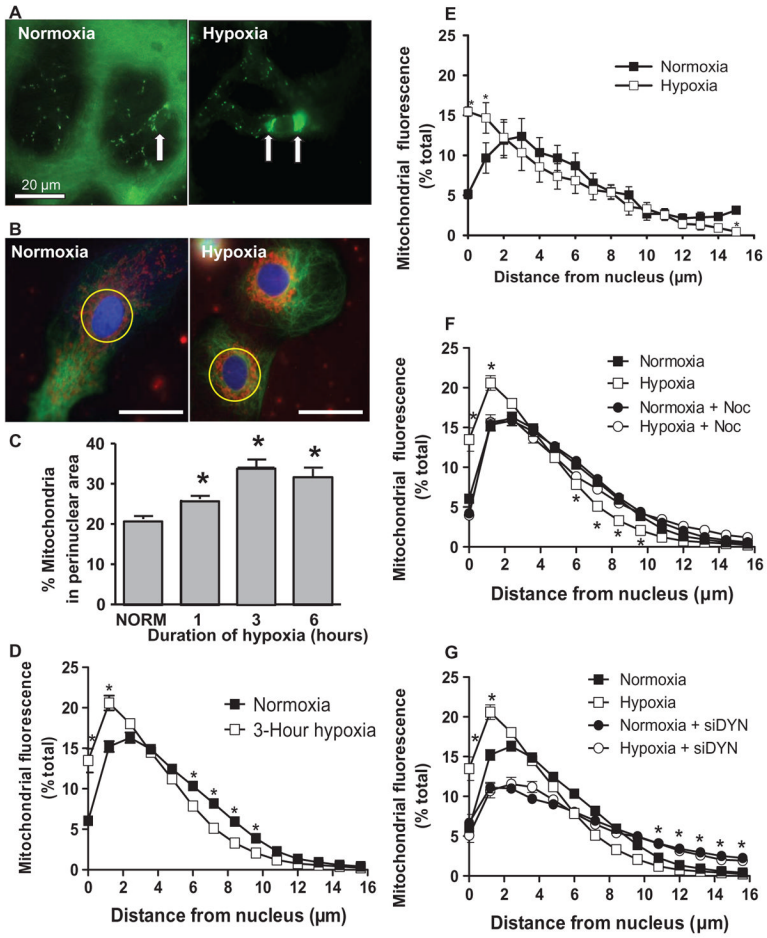

Fig. 1.

Perinuclear mitochondrial clustering in hypoxia: role of microtubules and the dynein motor system. (A) Left image: The arrow points to the nucleus of a capillary endothelial cell in a perfused rat lung. Mitochondrial labeling is green. Right image: Arrows point to clustered mitochondria after 3 hours of hypoxia. Scale bar, 20 μm. (B) Rat PAECs stained with MitoTracker Red, Oregon Green paclitaxel (microtubules), and Hoechst 33342 (nuclei, blue) were cultured under normoxia or hypoxia for 3 hours. Yellow circle denotes perinuclear region. Scale bar, 30 μm. (C) Quantification of perinuclear mitochondrial distribution in normoxic (NORM) and hypoxic PAECs. (D) Distribution of mitochondria in concentric rings radiating from the nucleus outward in normoxic and hypoxic PAECs. (E) Mitochondrial distribution in normoxic and hypoxic PASMCs. (F) Impact of the microtubule-destabilizing agent nocodazole (Noc) on mitochondrial distribution in normoxic and hypoxic PAECs. (G) Impact of siRNA knockdown of the dynein heavy chain (siDYN) on mitochondrial distribution in normoxic and hypoxic PAECs. $n = 6$ different culture dishes with three to six cells analyzed per dish. $*P < 0.05$, different from normoxia.

NIH-PA Author Manuscript
NIH-PA Author Manuscript
NIH-PA Author Manuscript

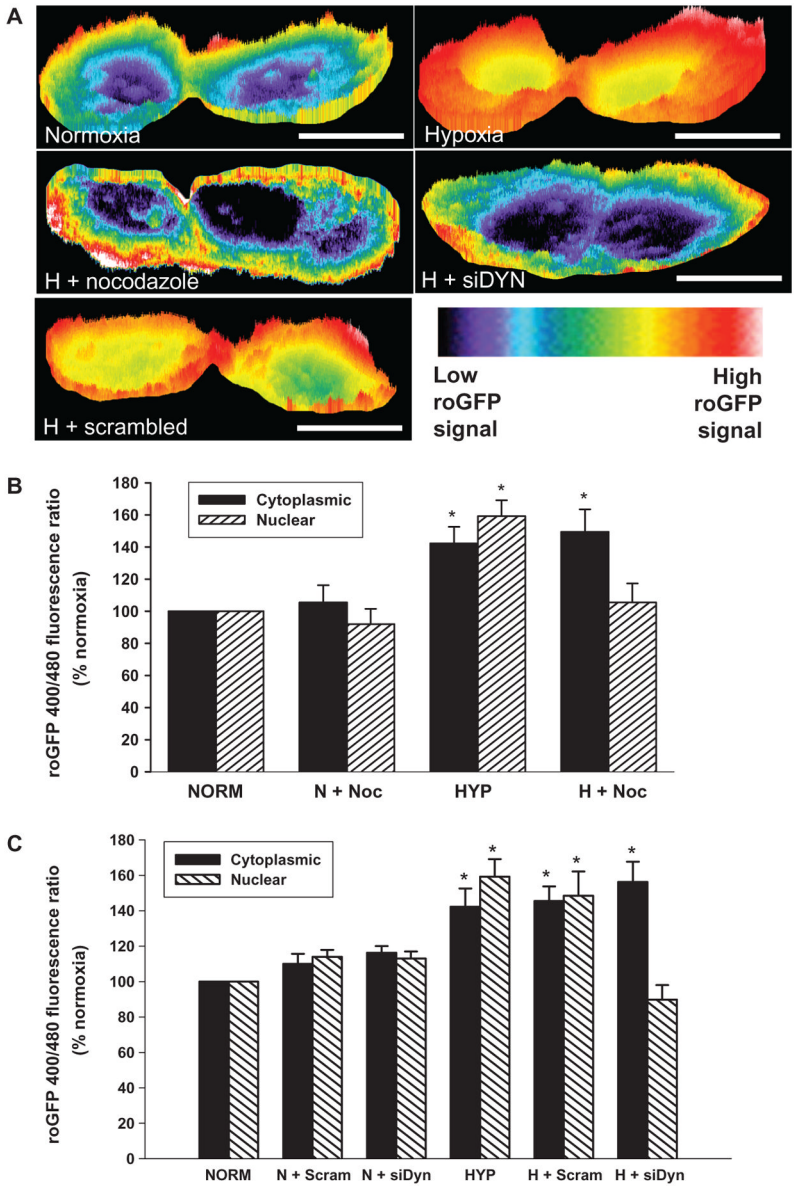

Fig. 2.

Impact of perinuclear mitochondrial clustering on hypoxia-induced pan-cellular ROS generation. (A) Pseudo-colored intensity plots of roGFP signal in normoxic PAECs and PAECs cultured in hypoxia (H) or cultured in hypoxia in the presence of nocodazole or after siRNA-mediated dynein knockdown (siDYN). roGFP signal intensity (indicated by the color bar) correlates with ROS concentrations. Scale bar, 15 μm. (B) Quantitative assessment of nuclear and cytoplasmic roGFP signals in the absence and presence of nocodazole (Noc) in normoxic (N) and hypoxic (H) PAECs. (C) Effect of dynein heavy chain–specific siRNA (siDYN) or scrambled siRNA (Scram) on hypoxia-induced changes in nuclear and cytoplasmic roGFP signals. $n = 3$ to 5 different culture dishes with three to six cells analyzed per dish for all panels. $*P < 0.05$, increased from normoxia.

NIH-PA Author Manuscript

NIH-PA Author Manuscript

NIH-PA Author Manuscript

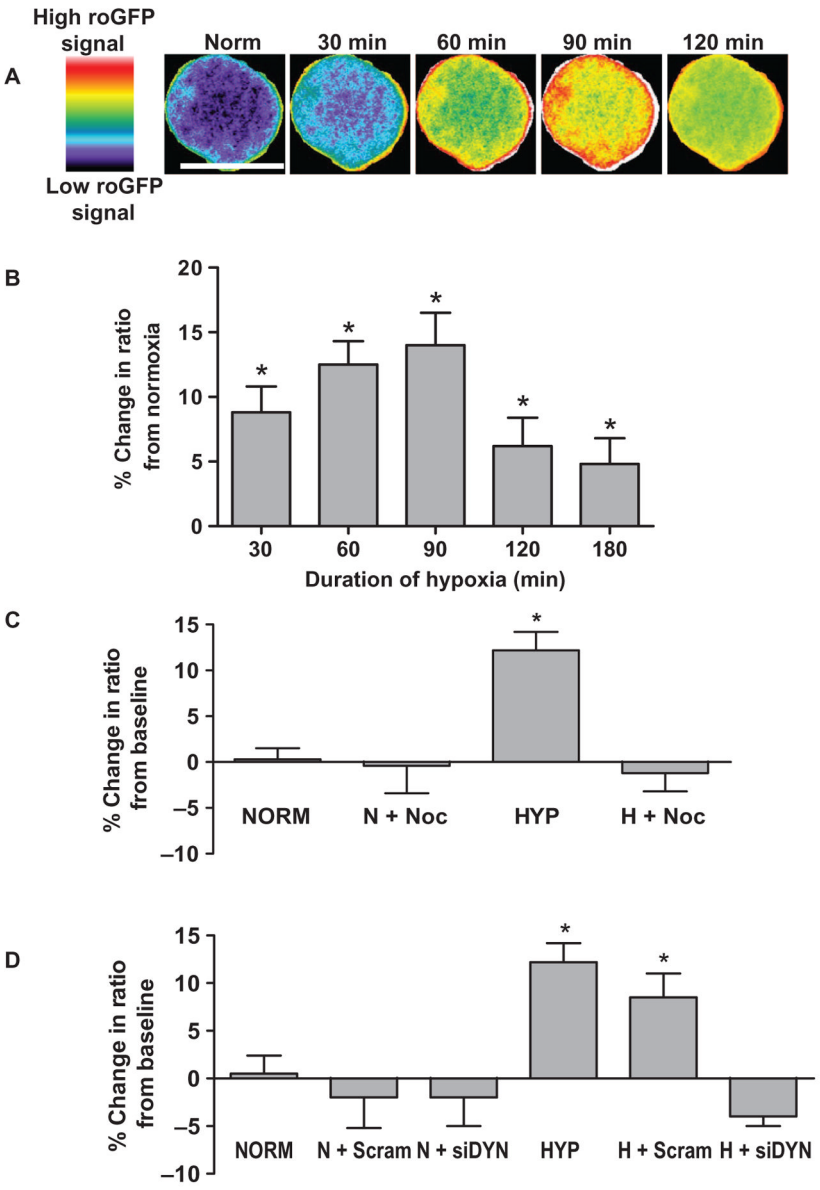

Fig. 3.

Hypoxia induces a redistribution of nuclear ROS that requires microtubule- and dynein-dependent perinuclear mitochondrial clustering. (A) Time-dependent effects of hypoxia on nuclear-targeted roGFP signals as depicted by pseudo-colored, ratiometric images of a PAEC nucleus. roGFP signal intensity (indicated by the color bar) correlates with ROS concentrations. Scale bar, 15 μm. (B) Time-dependent effects of hypoxia on nuclear roGFP fluorescence ratio in PAECs. (C) Effect of nocodazole on hypoxia-induced changes in roGFP fluorescence ratio in normoxic (NORM, N) PAECs and in PAECs cultured in hypoxia (HYP, H) for 60 min. (D) Effect of dynein-specific siRNA (siDYN) or scrambled siRNA (Scram) on roGFP fluorescence ratio in normoxic and hypoxic PAECs. $n = 3$ to 5 different culture dishes with 3 to 6 cells analyzed per dish for all panels. $^*P < 0.05$, increased from normoxia.

NIH-PA Author Manuscript

NIH-PA Author Manuscript

NIH-PA Author Manuscript

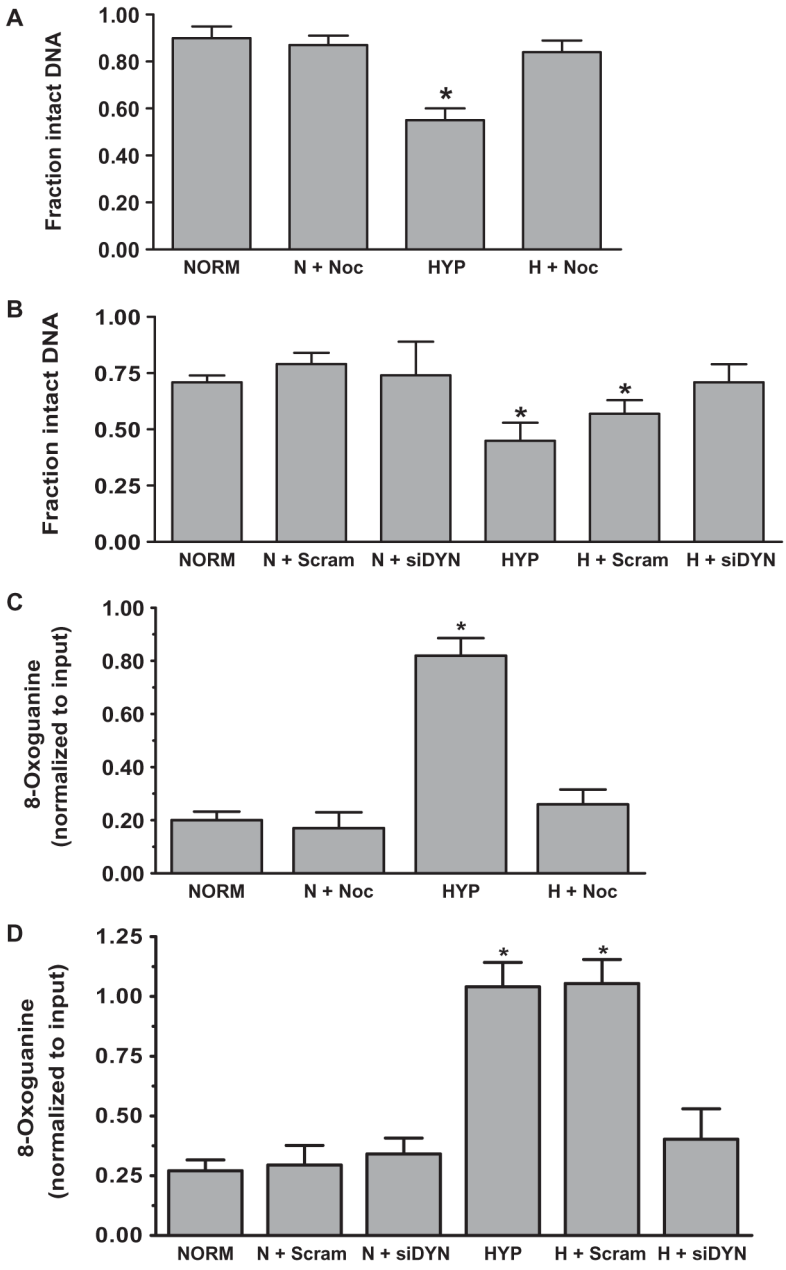

Fig. 4.

Hypoxia causes oxidative base modifications in the HRE of the *VEGF* promoter that require perinuclear mitochondrial clustering. (A) Effect of nocodazole on Fpg-detectable oxidative base damage in the *VEGF* HRE in PAECS cultured in normoxia (NORM, N) or hypoxia (HYP, H). (B) Effect of dynein-specific siRNA (siDYN) or scrambled siRNA (Scram) on Fpg-detectable oxidative base damage in the *VEGF* HRE in normoxic and hypoxic PAECS. (C) ChIP analysis of 8-oxoguanine–containing *VEGF* HRE sequences in PAECs treated with nocodazole. (D) ChIP analysis of 8-oxoguanine–containing HRE sequences in PAECs transfected with dynein-specific siRNA or scrambled siRNA. $n = 4$ to 6 different culture dishes for all panels. $*P < 0.05$, increased from normoxia.

NIH-PA Author Manuscript
NIH-PA Author Manuscript
NIH-PA Author Manuscript

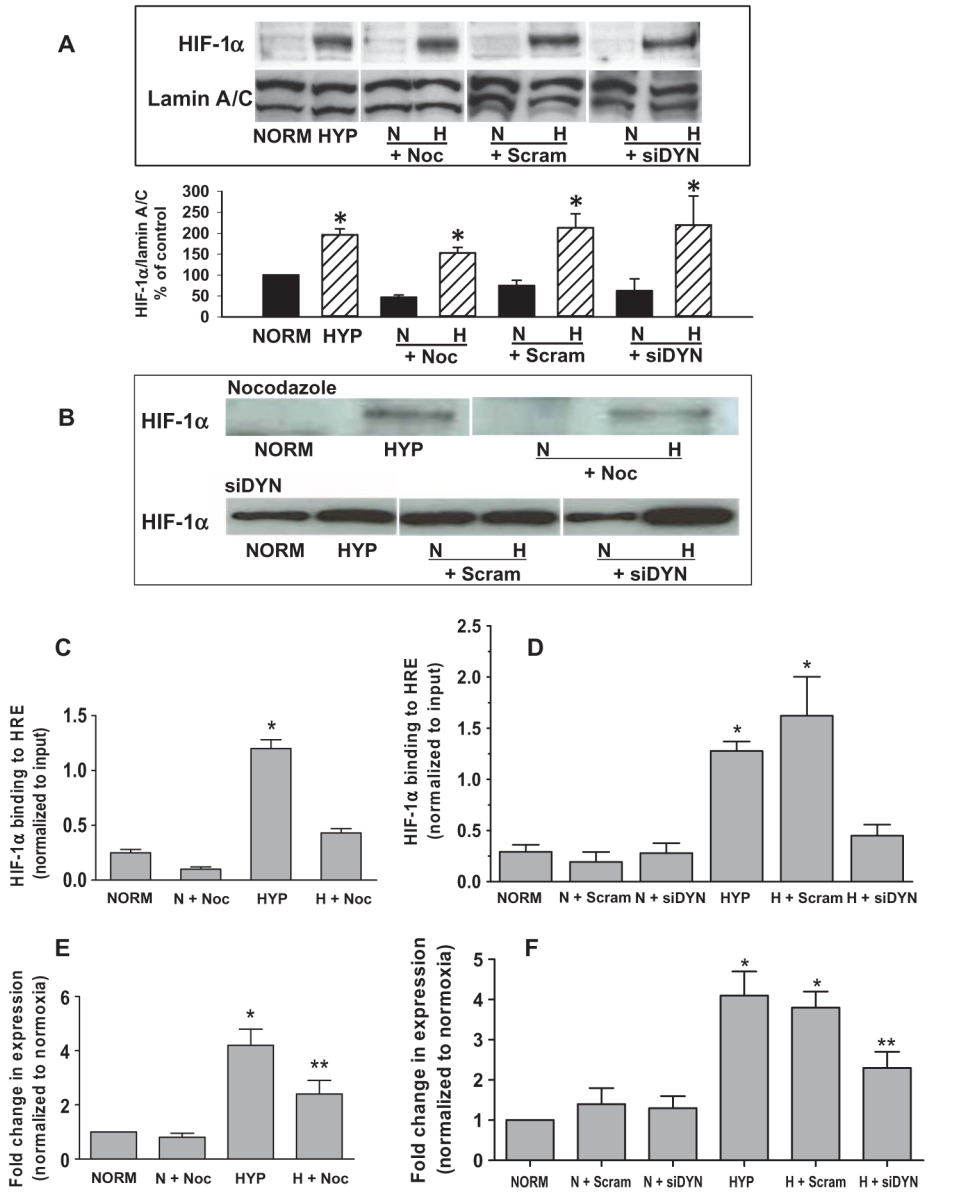

Fig. 5.

Base modifications in the *VEGF* HRE that occur after perinuclear clustering mitochondria are required for HIF-1α binding and *VEGF* mRNA expression. (A) Top: Western analyses of HIF-1α and the nuclear marker lamin A/C in PAECs cultured for 3 hours under normoxia (NORM) or hypoxia (HYP) in the presence of nocodazole (Noc) or after transfection with dynein-specific siRNA (siDYN). Representative of four experiments. Bottom: Quantification of HIF-1α abundance normalized to lamin A/C calculated as a percentage of the normoxic control. $n = 4$ separate culture dishes per experimental group. $^*P < 0.05$, increased from normoxia. (B) Western blot analysis of HIF-1α associating with a 65-mer oligonucleotide model of the *VEGF* HRE (DNA affinity precipitation analysis). Oligonucleotide-associated HIF-1α was derived from nuclear extracts isolated from normoxic and hypoxic control PAECs or PAECs treated with nocodazole or transfected with dynein-specific siRNA. Data are representative of three separate experiments. (C) ChIP analysis of *VEGF* HRE sequences immunoprecipitating with HIF-1α recovered from

NIH-PA Author Manuscript

NIH-PA Author Manuscript

NIH-PA Author Manuscript

PAECs incubated under normoxia or hypoxia in the presence of nocodazole. (D) ChIP assays for *VEGF* HRE sequences immunoprecipitating with HIF-1α from PAECs transfected with dynein-specific (siDYN) or scrambled siRNA (Scram). (E) Quantitative RT-PCR analysis of *VEGF* mRNA expression by PAECs in the presence of nocodazole. (F) Quantitative RT-PCR analysis of *VEGF* mRNA expression in PAECs transfected with dynein-specific or scrambled siRNA. $n = 4$ to 6 separate culture dishes per experimental group. $*P < 0.05$, increased from normoxia. $**P < 0.05$, different from normoxia and hypoxia alone.